Biochemical Pharmacology 162 (2019) 237–249

Contents lists available at ScienceDirect

Biochemical Pharmacology

journal homepage: www.elsevier.com/locate/biochempharm

Anti-tumor effect of sulfasalazine in neuroblastoma

Marie R. Mooney[a,1], Dirk Geerts[b], Eric J. Kort[a,c], André S. Bachmann[a,*]

[a] Department of Pediatrics and Human Development, College of Human Medicine, Michigan State University, 400 Monroe Ave NW, Grand Rapids, MI 49503, USA
[b] Department of Medical Biology, Amsterdam University Medical Center, University of Amsterdam, Meibergdreef 9, 1105 AZ Amsterdam, The Netherlands
[c] DeVos Cardiovascular Research Program, Spectrum Health and Van Andel Institute, 100 Michigan Ave. NE, Grand Rapids, MI, USA

ARTICLE INFO

Keywords:
Neuroblastoma
SPR
Sulfasalazine
Novel target
DFMO

ABSTRACT

Neuroblastoma (NB) is a tumor arising from the sympathetic nervous system during infancy and early childhood. High-risk patients who relapse often fail to respond to further therapy, which results in 5-year survival rate for this patient group below 5%. Therefore, there continues to be an urgent need for innovative treatments. Recently, we found that sulfasalazine (SSZ), an FDA-approved drug for the treatment of rheumatoid arthritis and ulcerative colitis induces anti-proliferative effects in NB tumor cells. SSZ was recently shown to inhibit sepiapterin reductase (SPR), a key enzyme that produces tetrahydrobiopterin (BH4) in the nitric oxide (NO) pathway. Here we tested SSZ against purified SPR *in vitro*, measured the anti-proliferative effect of SSZ on a panel of *MYCN* amplified and *MYCN* non-amplified NB cell lines, and assessed the anti-tumor effect of SSZ in NB tumor-xenografted mice. We found that the expression of both SPR mRNA and SPR protein was significantly higher in cell lines without *MYCN* amplification. SSZ inhibited SPR enzyme activity *in vitro* and exhibits anti-proliferative activity in a large number of NB cell lines derived from high-risk tumors. Importantly, oral/intraperitoneal (i.p.) SSZ co-administration resulted in measureable anti-tumor effects *in vivo*. The FDA-approved drug SSZ, a well-tolerated drug in clinical use, could be repositioned to inhibit tumor growth in NB.

1. Introduction

Neuroblastoma (NB) is a tumor arising from the sympathetic nervous system during infancy and early childhood [1]. Genetic biomarkers, most notable *MYCN* amplification, are used to stratify patients into risk categories, with low to moderate risk patients having positive outcomes exceeding 80% survival and high-risk patients facing a 50% survival rate despite aggressive, multimodal treatment [2,3]. Although treatments specific for NB, like ch14.18 antibody immunotherapy, are successful, no gene-targeting therapies, *e.g.* against MYCN, yet exist [4]. Patients with high-risk disease often relapse, at which point no curative therapy remains, resulting in a 5-year survival below 5%. The majority of high-risk and relapsed patients that do survive suffer late treatment effects resulting in severe challenges to their quality of life [5]. Therefore, these patients desperately need new therapeutic options, with higher efficiency, improved specificity, and lower toxicity. The most recent clinical advances consist of stem cell transplantation to prevent relapse and maintenance therapies administered after chemotherapy. Current maintenance therapy options include retinoic acid differentiation therapy and immunotherapy using either tumor-directed monoclonal antibodies or native immune system stimulators like cytokines and colony stimulating factors [3]. Our group has been instrumental in developing a forthcoming new maintenance therapy with α-difluoromethylornithine (DFMO) that arrests NB tumor cell proliferation and prevents tumor expansion [6–14]. Here we advance the understanding of another potential drug with this effect in NB *in vivo*: Sulfasalazine (SSZ).

SSZ is an FDA-approved drug used to treat rheumatoid arthritis and ulcerative colitis [15,16]. It is a rationally designed prodrug with an antimicrobial sulfonamide (sulfapyridine; SP) and an anti-inflammatory salicylic acid moiety (5-aminosalicylic acid; 5-ASA), linked by an azo bond [17]. Recently, the sulfonamide group in SSZ and related sulfa compounds was demonstrated to also function as an inhibitor of the enzyme sepiapterin reductase (SPR) [18]. SPR is an NADPH-dependent enzyme that metabolizes sepiapterin to tetrahydrobiopterin (BH4). BH4 is a critical cofactor for neuronal metabolism, required for both neurotransmitter anabolism and nitric oxide (NO) cell signaling. This vital role has been highlighted in patients with SPR deficiency, where SPR

Abbreviations: ATCC, American Type Culture Collection; DFMO, alpha-difluoromethylornithine; DMSO, dimethyl sulfoxide; BH4, tetrahydrobiopterin; NB, neuroblastoma; NO, nitric oxide; NOS, nitric oxide synthase; SPR, sepiapterin reductase; SRB, sulforhodamine B; SSZ, sulfasalazine

* Corresponding author.
E-mail address: andre.bachmann@hc.msu.edu (A.S. Bachmann).
[1] Current address: Duke University, School of Medicine, Center for Human Disease Modeling, Duke University, 300 N. Duke Street, Durham, NC 27701, USA.

https://doi.org/10.1016/j.bcp.2019.01.007
Received 18 October 2018; Accepted 8 January 2019
Available online 09 January 2019
0006-2952/

loss-of-function mutations in the central nervous system (CNS) result in Parkinson-like symptoms and cognitive impairments due to low BH4 levels and subsequently suppressed neurotransmitter production. In contrast, elevated BH4 levels have been implicated in NO-dependent processes supporting cellular proliferation or survival in endothelial cells, and in cancer cells including NB [19–23]. Since NO signaling acts as a rheostat, it produces pleiotropic effects on cells, variably inducing oncogenic proliferation and survival, or halting cell proliferation or inducing apoptosis, depending on its specific localization [24–26].

In this context, SSZ presents an interesting therapeutic option for NB, as it directly suppresses the SPR enzyme activity that supports BH4/NO production, resulting in lower cellular proliferation. Furthermore, the ability to modulate BH4 and NO production also influences NOS coupling and oxidative stress; in low BH4 conditions NOS enzymes (nNOS, iNOS, and eNOS, encoded by the *NOS1-3* genes, respectively) produce reactive oxygen species (ROS) rather than NO, and can induce cell death through either apoptosis or ferroptosis [27,28]. In addition, even though SSZ can cross the blood-brain barrier, as evidenced by anti-tumor and anti-depressive effects in brain cancer [29,30], it has already been used safely in humans for decades without producing symptoms of cognitive deficiency [15]. SPR inhibitors also successfully reduce neuropathic pain in peripheral nervous system (PNS) rodent models [31]. Considering the neuropathic pain NB patients often experience after chemotherapy [4], SSZ might also have a favorable profile for amelioration of treatment side-effects.

To investigate SPR inhibition as a potential NB therapy, our group has shown that reducing SPR enzyme levels in NB cells through siRNA knockdown [32] or SSZ treatment [33] suppressed cell proliferation *in vitro*. In the current work we show that a large number of NB cell lines derived from high-risk tumors are susceptible to SSZ treatment *in vitro*, and that oral/intraperitoneal (i.p.) SSZ co-administration exhibits measureable anti-tumor effects *in vivo*. While SSZ has previously been eschewed for the treatment of solid tumors due to its poor bioavailability, our results suggest that SSZ could be effectively repurposed for use in susceptible solid tumors like high-risk NB.

2. Materials and methods

2.1. Cell culture

Authenticated human NB cell lines were recently obtained from certified suppliers: LAN5 (Fisher Scientific, Waltham, MA, USA); KELLY, LAN1, SKNSH (Sigma, St. Louis, MO, USA); CHP134, CHP212, IMR32, SKNAS, SKNBE (ATCC, Manassas, VA, USA); SKNFI, SMSKAN, SMSKANR, SMSKCN, SMSKCNR (Children's Oncology Group, Lubbock, TX, USA). For SKNBE, the SKNBe(2)c clone (ATCC CRL-2268) was used. The cell lines MYCN2 and SHEP21N were provided by their inventors, Dr. Jason Shohet (Texas Children's Cancer Center, Baylor College of Medicine, Houston, TX) [34], and Dr. Manfred Schwab (German Cancer Research Center DKFZ, Heidelberg, Germany) [35], respectively. Cell lines were maintained in RPMI (Corning, Corning, NY, USA) containing 10% heat-inactivated fetal bovine serum (Hyclone by Fisher Scientific), penicillin (100 IU/ml), and streptomycin (100 µg/ml) in a humidified incubator at 5% CO_2 and 37 °C. Sulfasalazine (SSZ) was stored at 100 mM stock concentration in dimethyl sulfoxide (DMSO). Control cells were treated with 1% DMSO in culture medium, equivalent to the maximum amount of DMSO present at the highest doses of SSZ.

2.2. Cell viability

The sulforhodamine B (SRB) colorimetric assay (Sigma) was used to determine cell viability following SSZ treatment. Briefly, NB cells were plated in transparent flat 96-well plates and allowed to attach overnight. After exposure to SSZ (0, 75, 150, 300, 400, 500, 600, 700, 800, or 1000 µM), cells were fixed with 10% trichloroacetic acid (TCA) at 4°C overnight, washed with deionized water, and dried at room temperature. Cells were then stained with 100 µl 0.4% SRB in 1% acetic acid for 20 min at room temperature, rinsed five times with 1% acetic acid and allowed to dry at room temperature. One hundred µl of 10 mM Tris-HCl pH 7.0 was added to each well, shaken for 10 min at room temperature and read at 540 nm using a Biotek Synergy microplate reader. For cell viability during metabolite administrations, 100 mM stocks of SSZ, 5-ASA, and SP were made in 0.1 M hydroxide buffer and diluted in complete media for the drug exposure (0, 75, 150, 300, 400, 500, 600, 700, 800, or 1000 µM).

2.3. Western blot

For strongly adherent NB cell lines (CHP212, KELLY, MYCN2, SHEP21N, SKNAS, SKNBE, SKNFI, SKNSH), the culture medium was aspirated and the cells were washed 3 times with ice-cold phosphate buffered saline (PBS) prior to lysis with cold radioimmunoprecipitation assay (RIPA) buffer (20 mM Tris-HCl pH 7.5, 0.1% sodium lauryl sulfate, 0.5% sodium deoxycholate, 135 mM NaCl, 1% Triton X-100, 10% glycerol, 2 mM EDTA), supplemented with protease inhibitor cocktail (Roche, Basel, Switzerland). For loosely adherent NB cell lines (CHP134, IMR32, LAN1, LAN5, SMSKAN, SMSKANR, SMSKCN, SMSKCNR), the culture medium was collected, the remaining cells were gently washed with PBS and added to the collected medium, then the medium was centrifuged to form a cell pellet. The medium was aspirated, the pellet was washed with PBS, and again centrifuged prior to RIPA lysis. The adherent cells remaining on the plate were lysed in RIPA buffer with protease inhibitor. The lysates from plate and pellet were combined for protein analysis. Protein content was quantified with BCA reagent (BioRad, Hercules, CA, USA) on a Synergy H1 Biotek plate reader. Samples were diluted to equal protein concentration, and equal volumes were mixed with 4× Laemmli loading buffer (VWR, Radnor, PA, USA) and boiled for at least 5 min prior to loading on Tris-Glycine gels. The gels were transferred in 3-cyclohexylamino propanesulfonic acid (CAPS) buffer, pH 11.0 with 10% methanol, onto 0.4 µm PVDF membrane and blocked in 5% (w/v) milk powder in Tris-buffered saline with 0.1% Tween 20 (TBST) for 1 h at room temperature. Primary antibodies were diluted in 5% (w/v) BSA and applied overnight at 4 °C on an orbital shaker as follows: 1:500 SPR (ab157194, Abcam, Cambridge, MA, USA); 1:500 MYCN (sc-53993, Santa Cruz, Dallas, TX, USA); 1:1,000 GAPDH (4300, Ambion by Fisher Scientific). Targets were detected with Licor secondary antibodies at 1:10,000 dilution in 5% (w/v) milk powder in TBST on an Odyssey imager (Licor, Lincoln, NE, USA).

2.4. SPR enzyme purification

The SPR construct was a gift from Nicola Burgess-Brown (plasmid #39161, Addgene, Watertown, MA, USA). Using a PCR cloning approach, flanking BamHI and XhoI sites were added to the construct, which was then inserted into a pET24 expression vector containing GST fusion tag and HRV3C cleavage site immediately preceding the multiple cloning site. The construct assembly was confirmed by Sanger sequencing. For protein expression, LB with selective antibiotic was inoculated with bacteria containing the validated construct and incubated with shaking at 37 °C until the O.D. was 0.8. IPTG was added to 400 µM final concentration, and the culture was incubated overnight at 16 °C. Culture was then pelleted at 5000 *g* for 20 min, and resuspended with Cell Lytic B lysis buffer (Sigma) supplemented with protease inhibitors (cOmplete mini, EDTA free, Roche) and lysozyme (0.2 mg/ml). The lysate was incubated at room temperature for 15 min with shaking, and briefly sonicated to reduce viscosity. The lysate was cleared at 8000 *g* for 30 min. Cleared lysate was incubated with washed glutathione resin for 4 h at 4 °C with rotation. The resin was then washed three times with PBS, and once with HRV 3C buffer from the HRV 3C protease kit (Fisher Scientific). The resin was resuspended in HRV 3C buffer and HRV3C enzyme was added (60 U/ml). Cleavage was allowed to proceed

overnight at 4 °C with rotation. The resin was pelleted and cleaved SPR protein was transferred to a new tube and stored at −20 °C as a 50% glycerol suspension.

2.5. SPR activity assay

The SPR activity assay was performed as previously reported [36]. Briefly, 200 µl reactions were carried out in a 96-well plate with the standard reaction mixture (100 mM potassium phosphate buffer pH 6.2, 50 µM L-sepiapterin) and 2 µg of purified human SPR enzyme, with or without 1 mM SSZ or 1 mM DMSO vehicle control. The reaction was started by adding NADPH (100 µM final concentration) and measured by absorbance decrease at 420 nM. Readings were normalized to the appropriate control; the standard reaction mixture without the SPR enzyme and with or without SSZ. SSZ interferes with the absorbance reading at 420 nM and thus requires a separate control. Enzyme activity was determined from the linear part of the reaction curve using the coefficient of extinction for sepiapterin ($\varepsilon = 10.4\ mM^{-1}\ cm^{-1}$). With cell lysates, cells were pretreated with drug (200 µM SSZ) for either 2 h or overnight prior to lysate collection. Total protein was equalized to 25 µg/ml for use in the assay.

2.6. Nitric oxide determination

Release of nitric oxide (NO) from cells was determined with the Griess assay. SKNBE cells were plated at 32,000 cells per well in a 96-well plate and allowed to adhere overnight, then pretreated for 2 h with 1 mM SSZ. NO was induced with 10 ng/ml IL-6 for 24 h, then 100 µl medium was collected into a new plate with equal volume of Griess-Ilosvay's nitrite reagent (109023, Millipore, Burlington, MA, USA). After 30 min, absorbance increase at 520 nm was recorded as measure of NO presence.

2.7. Semi-quantitative polymerase chain reaction (PCR)

PCR was carried out using the manufacturer protocol for 2× Mean Green master mix (Empirical Biosciences, Grand Rapids, MI, USA) with the primers (5′– > 3′): MYCN-F CAGTCGGCGGGAGTGTTG; MYCN-R CTCGAGGTCTGGGTTCTTGC; SPR-F TATCAACAACGCGGGCTCT; SPR-R GAAGTCAGGCAGAGCATGGA; SDHA-F ACTGTTGCAGCACAGCTA GAA; SDHA-R GCCCTTTCCAAACTTGAGGC. SDHA was chosen as a loading control instead of GAPDH, considering the known transcriptional co-regulation between MYCN and GAPDH in NB [37].

2.8. In vivo tumor xenograft studies

The animal study was performed at the Van Andel Research Institute (VARI, Grand Rapids, MI, USA) and approved by the VARI Institutional Animal Care and Use Committee (IACUC). The *MYCN*-amplified NB cell line SKNBE was xenografted into the right flank of male athymic nu/nu mice (available at VARI). Cells were suspended in a 50% PBS, 50% Culturex BD matrigel solution and implanted at a concentration of 50,000 cells in 100 µl per animal. Up to four individual mice were housed per cage and supplied with Medidrop sucralose liquid gel (ClearH20, Westbrook, ME, USA) instead of water in red translucent bottles. Animal weight and fluid intake were monitored three times per week. Cages of tumor-bearing animals were assigned to control and treatment arms in the following way to control for initiating treatment on asynchronously developing tumors within a cage: once an individual tumor became measurable by digital calipers (> 50 mm^3), the cage was assigned to the control group if any additional mice in the cage did not have palpable tumors, whereas the cage was assigned to whichever arm had fewer individuals assigned if all of the additional mice housed in that cage did have palpable tumors. Control animals continued to receive Medidrop water with 0.5% carboxymethylcellulose (CMC) added as a vehicle. Treatment animals were initially provided with Medidrop solution containing 0.5% CMC and 36 mg/ml SSZ. Due to a reduction in fluid intake at this concentration, the bottles were replaced with 3.6 mg/ml SSZ on day 2–3 of treatment, and this dose was maintained for the rest of the study. Animals also received a daily intraperitoneal (i.p.) injection of 150 mg/kg SSZ, 6 h into the vivarium light cycle when animal activity and fluid intake was low. This dose was approximately equivalent to the maximum expected ingested dose from a single drinking session, assuming a maximum of 6 ml water ingested per animal per day in at minimum 8 drinking sessions. The SSZ for i.p. injections was made fresh weekly and stored away from light in the refrigerator. Tumors were measured by digital calipers three times a week during the study. Once tumor size exceeded 1500 mm^3, animals were euthanized and tumor tissue collected.

Table 1
NB cell line sensitivity to SSZ.

Cell Line	*MYCN* status	SSZ IC-50 (µM)	95% confidence interval (µM)
SHEP21N	Tet-off	~154	Very wide
MYCN2	Tet-on	375	270–522
SKNAS	−	537	344–838
SKNFI	−	> 1000	Not reached
SKNSH	−	> 1000	Not reached
IMR32	+	400	353–453
KELLY	+	523	342–801
CHP134	+	322	293–353
CHP212	+	> 1000	Not reached
LAN1	+	> 1000	Not reached
LAN5	+	> 1000	Not reached
SKNBE	+	378	270–420
SMSKAN	+	350	322–389
SMSKANR	+	289	220–381
SMSKCN	+	436	299–637
SMSKCNR	+	233	177–306

Cell viability determined by the SRB assay in response to SSZ administration in 16 cell lines. IC-50 values are determined on triplicate independent experiments (n = 3) from each cell line and a non-linear regression fit with four parameters, except for the cell lines CHP212, LAN1, LAN5, SKNAS, SKNFI, and SKNSH where a three parameter fit was applied because the treatment did not maximally inhibit cell viability at the highest doses. SHEP21N and MYCN2 are NB cell lines that contain MYCN under control of tetracycline-regulated promoters. SHEP21N has a tet-repressible ("Tet-off") promoter, MYCN2 contains a tet-inducible ("Tet-on") promoter. Addition of tetracycline/doxycycline leads to MYCN repression or MYCN expression in SHEP21N or MYCN2, respectively. All cell lines were grown under typical culture conditions without tetracycline/doxycycline.

Table 2
SPR-NOS mRNA expression correlations in NB tumors.

Gene combination	Correlation	P value
SPR-NOS1	0.139	$1.90{\cdot}10^{-3}$
SPR-NOS2	0.165	$2.20{\cdot}10^{-4}$
SPR-NOS3	0.129	$3.90{\cdot}10^{-3}$

SPR mRNA expression correlations with the three NOS genes in NB tumors. The SEQC-498 RNASeq dataset was queried for SPR and NOS gene mRNA expression, and correlation significance was determined using a 2logPearson correlation test. Shown are correlations for the predominant mRNA splice variants for each NOS gene: NOS1 (NM_000620.4, isoform 1), NOS2 (NM_000625.4), NOS3 (NM_000603.4, isoform 1). For details on dataset analysis see Materials and Methods.

2.9. Histologic analysis

Fixed tissues were paraffin embedded, sectioned, and mounted on slides for hematoxylin-eosin (H&E) staining and immunohistochemistry (IHC); antibodies used were SPR (ab157194, Abcam) at 1:300 dilution and uNOS (E3932, detects all three NOS proteins, Spring Biosciences, San Jose, CA, USA) at 1:75 dilution.

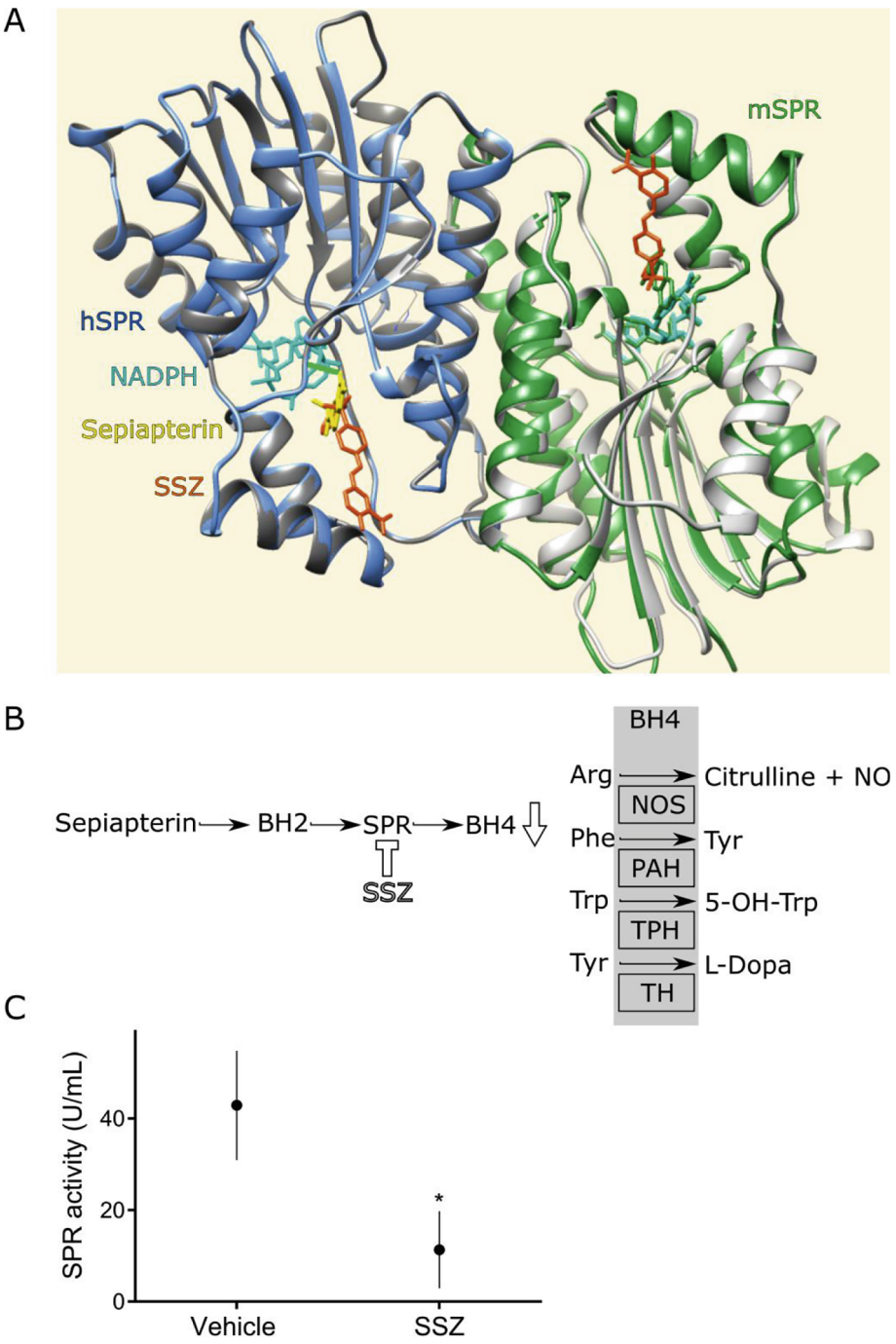

Fig. 1. Model of SSZ effects on SPR. (A) Superimposed crystal structures of SPR either with its ligand sepiapterin, derived from the mouse SPR structure PDB SEP1 (mSPR), or with SSZ, derived from the human SPR structure PDB 4J7X (hSPR). Sepiapterin binding to hSPR and SSZ binding to mSPR are modeled with Swiss Dock. (B) Schematic of SPR metabolic pathway production of the BH4 cofactor required for several downstream enzymes. (C) SPR *in vitro* activity using purified enzyme, with and without SSZ.

2.10. NB public mRNA expression dataset analysis

Expression data from the public human NB cell line mRNA expression dataset Versteeg-24 (GSE28019) and the human NB tumor mRNA expression dataset SEQC-498 (GSE62654, the largest public NB tumor RNA sequencing dataset) were retrieved from the NCBI GEO website (http://www.ncbi.nlm.nih.gov/geo/) and analyzed using the R2 genomics analysis and visualization platform (developer Jan Koster, Department of Oncogenomics, Amsterdam University Medical Center, The Netherlands) at (http://r2.amc.nl). Versteeg-24 data were analyzed as in [38]: gene transcript levels were determined using GeneChip operating software (MAS5.0 and GCOS1.0, from Affymetrix, Santa Clara, CA, USA), and samples scaled to an average intensity of the middle 96% probe-set signals to 100 for every sample, to enable comparisons between samples. SEQC-498 dataset mRNA expression levels were determined by sequence alignment to human RefSeqs using the R2 TranscriptView tool and transcript counting. All details for the datasets used is available using the GSE identifiers on the NCBI GEO website. All analysis of human material and data complied with the "Declaration of Helsinki for Medical Research involving Human Subjects" (http://www.wma.net/en/30publications/10policies/b3/index.html) and was with approval from the Amsterdam University Medical Center research

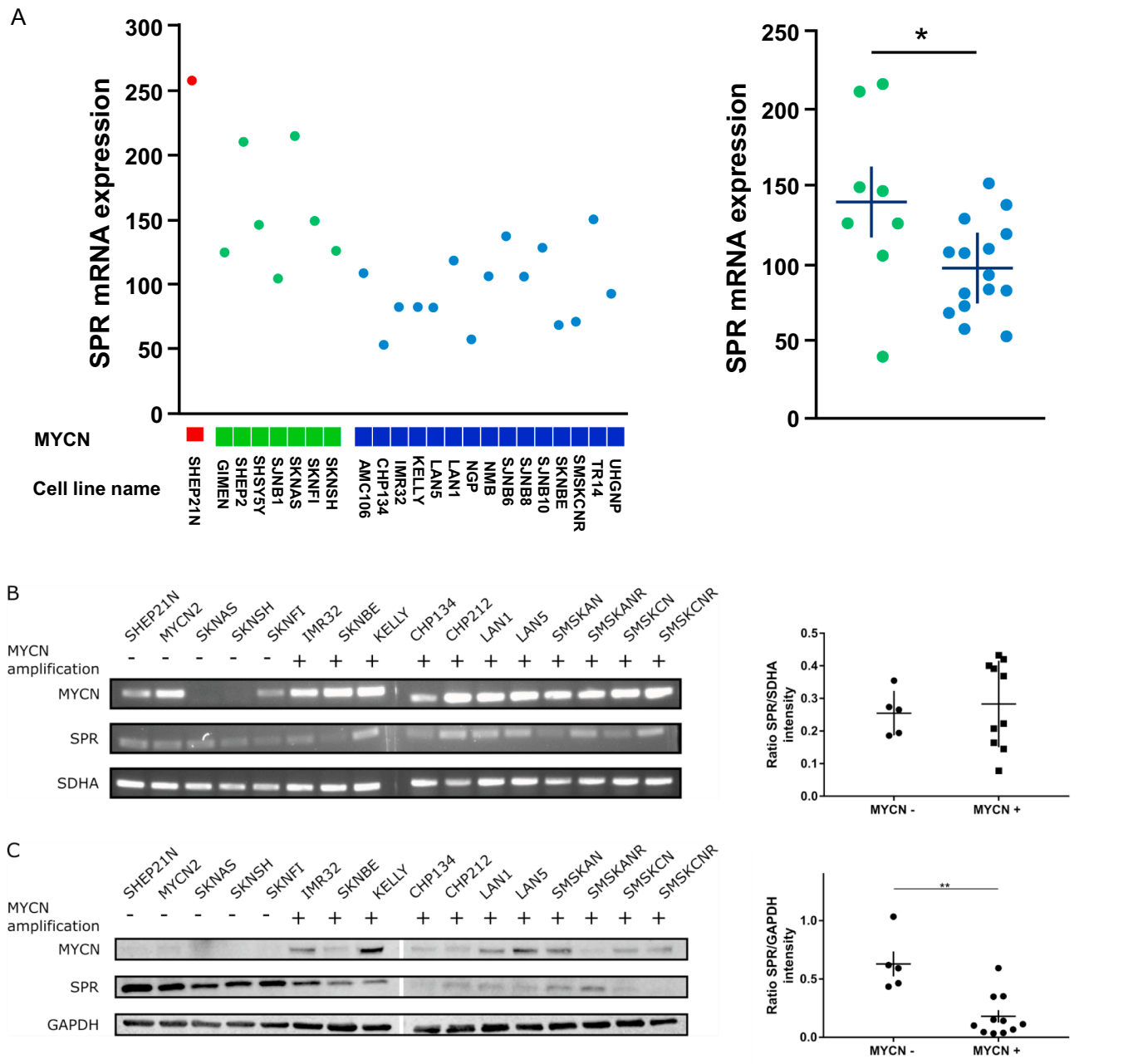

Fig. 2. SPR is expressed in NB cell lines and inversely correlates with MYCN expression. (A) SPR mRNA expression values from the Versteeg-24 public dataset in R2, with significantly higher expression in cell lines without *MYCN* amplification than in cell lines with *MYCN* amplification (ANOVA, $p < 0.05$). (B) SPR mRNA expression as determined by testing (an overlapping) series of NB cell lines by semi-quantitative PCR. (C) SPR protein expression levels as determined by Western blot with SPR protein significantly higher expressed in cell lines without *MYCN* amplification (Mann-Whitney rank sum, $^{**}p < 0.01$).

and ethics committee "Medisch Ethische Commissie (MEC)". Expression data (CEL files) R2 TranscriptView was used to verify that probe-sets had a unique anti-sense position in a late coding exon or the 3' UTR of the gene. The probe-sets selected for this study all meet these criteria.

2.11. Statistical analyses

Statistical analysis on the SPR expression data in Versteeg-24 (Fig. 2A) was performed using an ANOVA test in R2. Densitometry for Western blots (Fig. 2C) was performed using GelAnalyzer to calculate the intensity area under the curve with rolling ball background correction set to 35. We applied the Mann-Whitney rank sum test between *MYCN* non-amplified and *MYCN* amplified cell lines using the ratio of SPR to GAPDH for each cell line in triplicate. IC-50 plots (Fig. 3 and Table 1), tumor size regression analysis (Fig. 6B), and Kaplan-Meier plots (Fig. 6C) were generated in GraphPad Prism (version 5.04, GraphPad). The IC-50 was determined from a non-linear regression fit with four parameters, except for the cell lines CHP212, LAN1, LAN5, SKNAS, SKNFI, and SKNSH where a three parameter fit was applied because the treatment did not maximally inhibit cell viability at the highest doses. For *in vivo* studies, day zero represents the day when tumors were first measureable for each animal, resulting in asynchronous measurement intervals for the tumor size, so the tumor volumes are represented with the last-observation-carried-forward until the tumor size exceeded euthanasia threshold at 1500 mm^3. Once a tumor exceeded euthanasia criteria, the animal was censored from the group, and once either group no longer comprised three uncensored animals, the tumor growth rates were estimated by a linear regression fit, and an

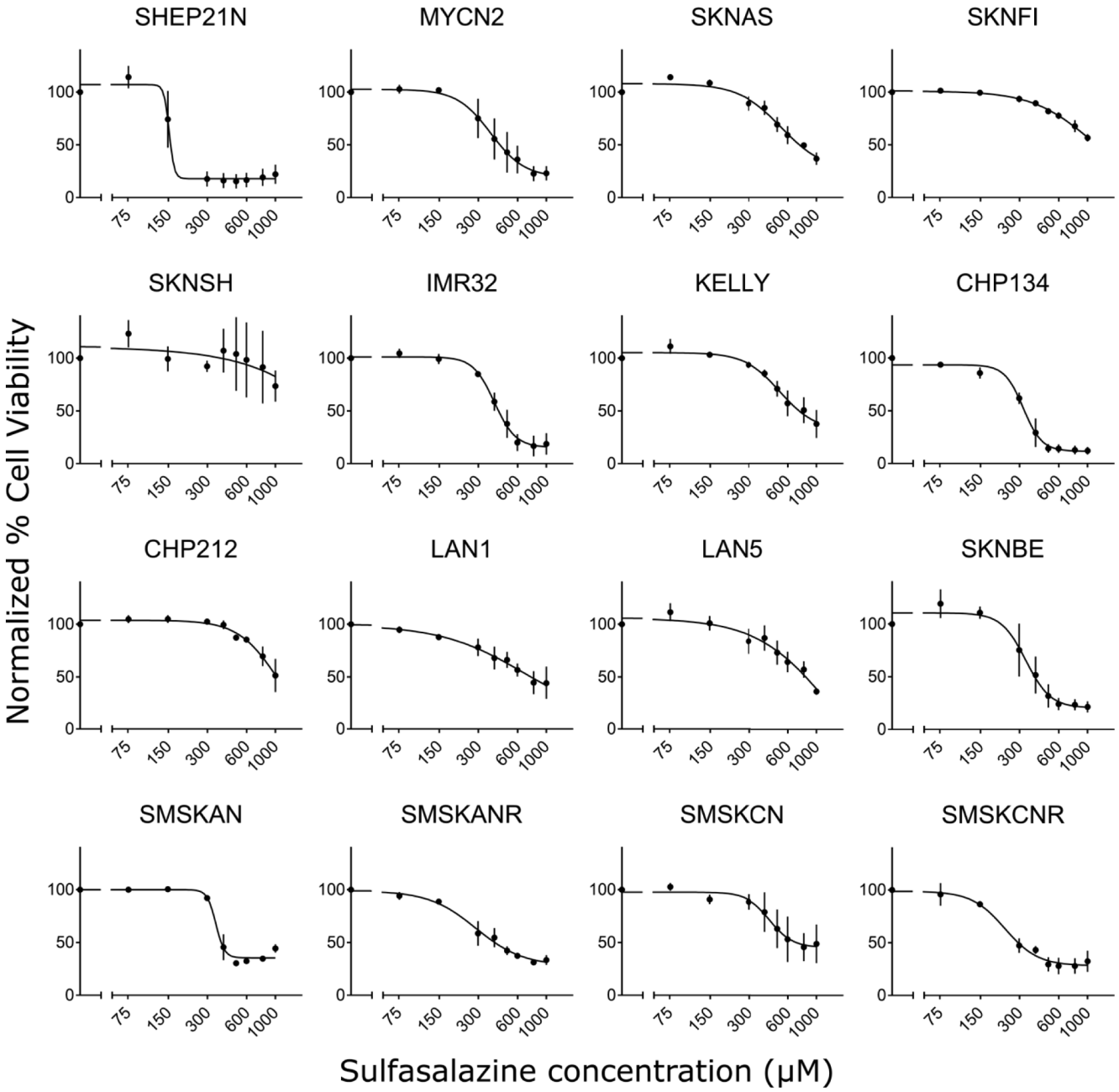

Fig. 3. High-risk, *MYCN* amplified NB cell lines are sensitive to SSZ. Optimal cell plating densities for each cell line were determined empirically. Cells were plated at optimal density and treated the next day with SSZ (0, 75, 150, 300, 400, 500, 600, 700, 800, or 1000 μM) for 72 h. The cells were then fixed with a final concentration of 10% TCA for the SRB cell viability assay. Data are represented as percent (%) inhibition compared to untreated cells from three independent replicates (n = 3) ± standard error (S.E.).

F-statistic was used to determine whether the mean tumor growth rate was different between the control and treatment arms. Differences in mouse survival were determined with a Kaplan-Meier Log-Rank analysis, using the tumor size threshold as the endpoint. SPR-NOS gene mRNA expression correlations (Table 2) were calculated with a 2log Pearson test. The significance of a correlation is determined by t = R/sqrt((1 − r^2)/(n − 2)), where R is the correlation value and n is the number of samples. Distribution measure is approximately as t with n − 2 degrees of freedom. Gene tumor mRNA expression correlation with survival probability (Fig. 8B) was evaluated by Kaplan–Meier analysis using the log-rank test as described [39]. To determine the optimal value of gene expression to set as cutoff value, all tumor samples were first sorted according to gene mRNA expression and subsequently divided into two groups. For each group separation (higher or lower than the current expression, minimum group size n = 8), the log-rank significance was calculated. The best P-value obtained was used to represent the final gene expression cutoff value. To correct for multiple testing, the resulting P-value was divided by the number of tests performed (n − 16, Bonferroni correction). This procedure was called Kaplan Scan. In addition, analyses were performed on groups separated by median or average tumor mRNA expression values. For all tests, a value of $P < 0.05$ was considered statistically significant.

2.12. Structure modeling

The human structure of a dimeric SPR complex is represented in gray. One subunit is superimposed with the human SPR structure (blue)

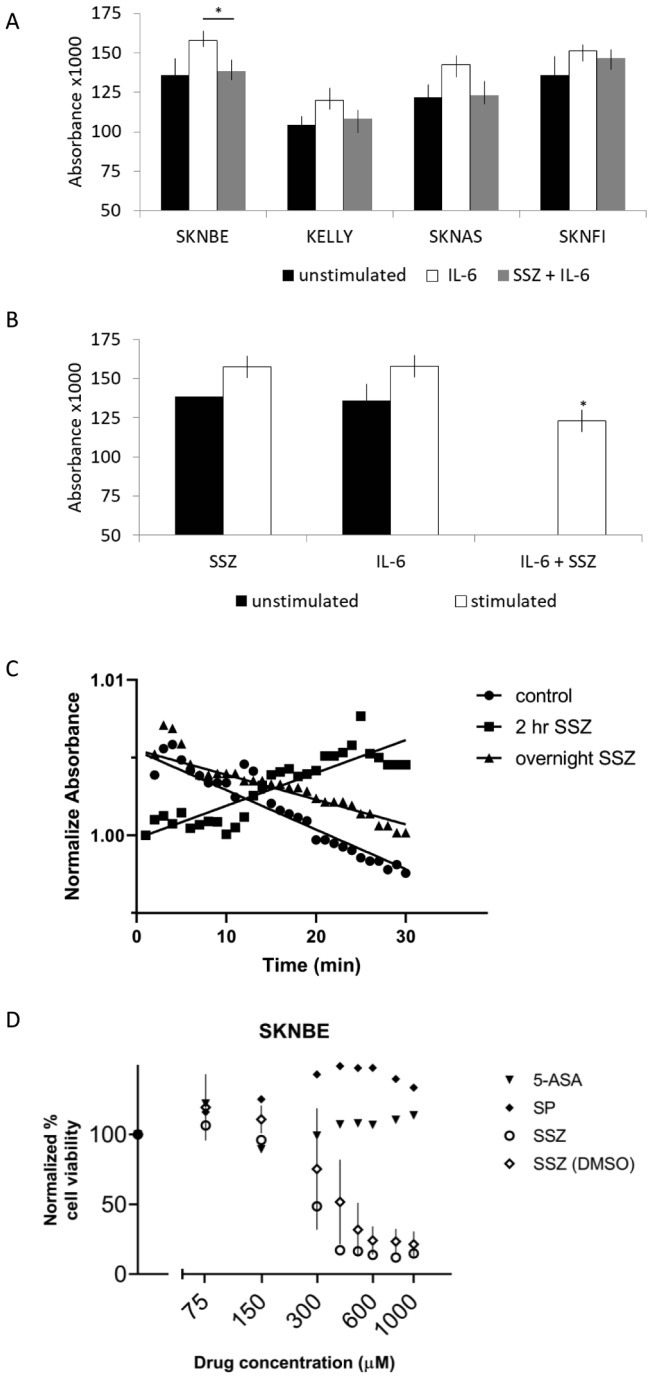

Fig. 4. Cellular responses to stimuli, SSZ, and SSZ metabolites. (A) NO production in SKNBE cells pretreated with 1 mM SSZ for 2 h and then induced by 10 ng/ml IL-6 over 24 h. (B) Induced NO inhibition. $^{*}p < 0.05$, single-tail *t*-test, for combination compared to single agent. The unstimulated and SSZ alone experiments were conducted independently of the other conditions (which appear with other cell lines in panel A), and have been scaled to the average value of the control condition for panel A. (C) Inhibition of SPR enzyme activity by SSZ (200 μM) in lysates of SKNBE cells. D) Sensitivity to SSZ metabolites. SRB cell viability assay normalized to solvent control (100× drug stock in 0.1 M hydroxide). SSZ in DMSO (from Fig. 3) is included for comparison.

loaded with NADPH (cyan) and SSZ (red) from PDB 4J7X [40]. As the natural ligand for the human structure has not been co-crystallized, we approached structure definition by docking sepiapterin (yellow) with the human structure using Swiss Dock (conformation #20, http://www.swissdock.ch/) [41]. The second human SPR unit is aligned with the mouse structure loaded with NADPH and the natural ligand biopterin (all dark green; PDB SEP1 [42]) to guide the choice of docking position for sepiapterin in the human structure.

3. Results

3.1. Model for SSZ anti-tumor effects through interaction with SPR

Elevated SPR and BH4 levels contribute to tumor growth and survival [32,33,43]. To understand how SSZ inhibits SPR activity, we superimposed the crystal structure of SPR with its natural ligand (PDB SEP1) [42] or with SSZ (PDB 4J7X)[40] and concluded that SSZ likely competes with the ligand for the active site, thus reducing BH4 availability for neurotransmitter anabolism and NO production (Fig. 1A, B). We had previously proposed that SSZ would bind with SPR at its NADP + -binding site and thus might potentially affect NADP + -dependent proteins [33]. The unpublished human crystal structure (PDB 4J7X) used in this model shows SSZ binding adjacent to NADP +, where ligand binding is predicted instead, potentially limiting the number of SSZ-affected proteins. SSZ and other sulfamide-containing compounds have previously been reported to inhibit SPR enzyme activity [18]. For verification, we performed a SSZ inhibition study with purified SPR and confirmed that SSZ inhibits SPR activity in our experimental settings (Fig. 1C).

3.2. SPR is expressed in NB tumor cell lines

To determine the presence of SPR as a target in a variety of NB cell lines, we examined SPR expression using public and empirical data. At the mRNA expression level, R2 public microarray profiling data from the Versteeg-24 NB cell line dataset suggests moderate, but widespread mRNA expression for all cell lines investigated (Fig. 2A). SPR mRNA expression was significantly higher in cell lines without *MYCN* amplification than in cell lines with *MYCN* amplification. We tested a substantial number of these cell lines by semi-quantitative PCR and found similar results (Fig. 2B). We also analyzed SPR protein expression in this latter NB cell line series (total of 16 cell lines) by Western blot (Fig. 2C). Indeed, SPR protein was also widely expressed in the NB cell lines. Protein expression levels appeared to show higher variability than mRNA expression (data not shown). Similar to SPR mRNA, SPR protein expression is significantly higher in cell lines without *MYCN* amplification (Mann-Whitney Rank Sum, $p < 0.01$). The results confirm that SPR is expressed in NB cell lines and that these lines are suitable to test the effect of SSZ.

3.3. NB tumor cell lines are sensitive to SSZ

To assess the anti-proliferative effect of SSZ against a variety of NB cell lines, we calculated the IC-50 response to SSZ for 16 cell lines. We had previously tested the *MYCN* amplified NB cell lines LAN5 and SKNBE for SSZ sensitivity [33]. Here, we extend that analysis to a larger panel of *MYCN* amplified cell lines, as well as to cell lines without *MYCN* amplification. We show that 10 of 16 cell lines tested demonstrate a similar sensitivity to SSZ, with an IC-50 value averaging ~400 μM SSZ across the sensitive cell lines (Fig. 3). The IC-50 values for each cell line with their 95% confidence intervals are summarized in Table 1. While 400 μM is generally a very high concentration for most anticancer compounds, we note that the safe clinical use of SSZ in humans ranges from a typical dose of 1–4 g daily, with a maximal tolerated dose of 12 g daily for non-cancerous conditions [44]. Sensitivity to SSZ did not necessarily correlate with SPR mRNA or protein expression, but cell lines without *MYCN* amplification (SKNAS, SKNSH, and SKNFI), though limited in number, were generally more resistant to SSZ treatment.

In anticipation of testing SSZ *in vivo*, we measured drug-associated downstream responses in cell lines. NO production in cell lines that

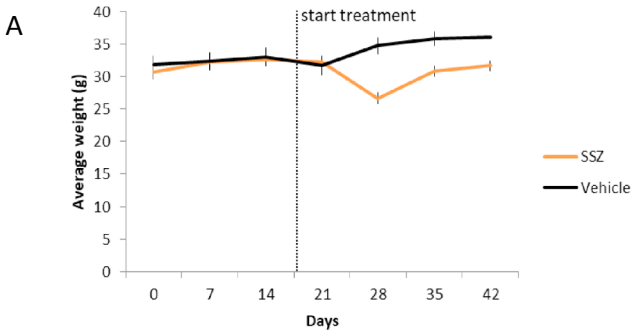

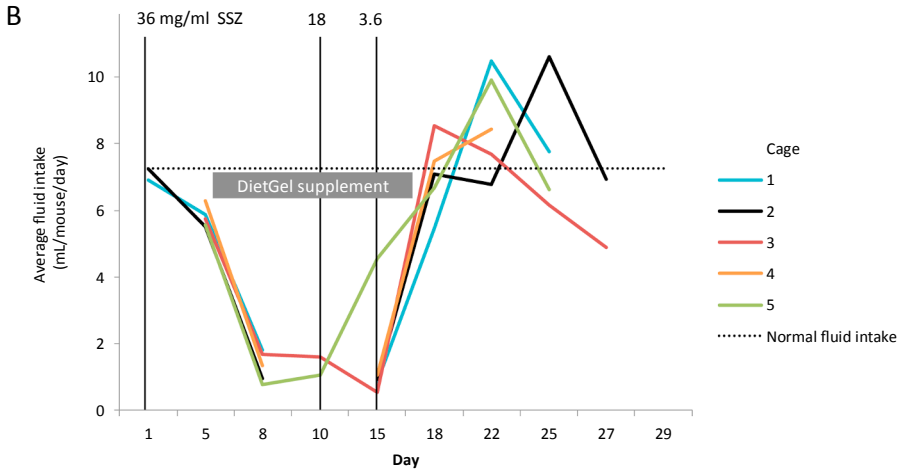

Fig. 5. Maximum tolerated dose of SSZ in drinking water in mice. (A) Average weight (g) of mice and (B) average fluid intake (mL/mouse/day) of SSZ Medidrop solution during treatment. Previous reports suggested that SSZ could be supplied in drinking water at concentrations up to 150 mg/mL [50]. In order to keep the animals hydrated and drinking normal amounts of fluid without weight loss, we supplemented animals with DietGel and reduced the SSZ concentration until intake returned to normal.

were pretreated with SSZ and then induced by IL-6 showed a tendency toward NO inhibition which was strongest in SKNBE and less pronounced in MYCN non-amplified and SSZ insensitive cell lines ($p = 0.055$, Fig. 4A, B). In addition, we confirmed that SSZ inhibits SPR enzyme activity also in lysates of SKNBE cells (Fig. 4C). Furthermore, the SSZ metabolites 5-ASA and SP did not illicit a reduction in cell viability in SKNBE cells (Fig. 4D). Collectively, these results suggest that SKNBE cells are sensitive to SSZ and suitable for *in vivo* NB tumor xenograft mouse studies.

3.4. SSZ reduces the growth rate of NB tumor xenografts in nude mice and improves survival

To test SSZ efficacy in an *in vivo* NB model, we established a protocol using the SSZ-sensitive NB cell line SKNBE, which also demonstrated SPR inhibition and trended toward NO responsiveness *in vitro* (Fig. 4). SSZ has a well-established pharmacokinetic and pharmacodynamics profile in mice and humans [45,46], demonstrating that high doses of the drug can be administered safely. However, SSZ also has poor tissue adsorption and a short half-life, requiring that the maximum tolerated dose be administered. For these reasons, SSZ use in a clinical cancer setting prioritizes accessible tumor types of the gastrointestinal tract [47,48], and SSZ has only recently been considered for pre-clinical testing in some less accessible solid tumors (prostate cancer [49], pancreatic cancer [50,51], breast cancer [52], hepatocellular carcinoma [53], and glioma [54,55]). The results from those studies have been mixed, but since we have previously observed a similar drug profile with DFMO that nonetheless inhibited NB growth, we moved forward with testing SSZ drug effects in mice harboring subcutaneous SKNBE xenografts.

Tumor-bearing mice were randomly assigned to control and treatment arms once tumors became measureable and SSZ was administered at a maximal dose of 3.6 mg/ml in the drinking water to maintain drug exposure over time. Drug ingestion and animal weight measures were recorded (Fig. 5). In addition, we also administered a daily i.p. injection of 150 mg/kg SSZ 6 h into the vivarium light cycle, when the mice are less active and do not ingest as much drug via the drinking water. Control animals experienced aggressive tumor growth, whereas tumor growth inhibition occurred in SSZ-treated animals (Fig. 6A). The growth rates were compared from a linear regression fit of the data, showing a much lower growth rate in the SSZ-treated group ($^{***}p < 0.001$, Fig. 6B) that coincided with a doubling of the animal survival time until the tumor burden exceeded the threshold for euthanasia ($^{**}p < 0.01$, Fig. 6C).

3.5. SPR and NOS mRNA are expressed in vivo and correlate with poor clinical prognosis

To further examine the *in vivo* anti-proliferative effects of SSZ, we performed tissue staining on our xenograft tumors. The tissues did not reveal any difference in ki67 or cleaved caspase staining (Fig. 7), both of which have been observed before in other applications of SSZ and have been attributed to cells delaying cell cycle progression rather than undergoing senescence [54,56], and undergoing ferroptotic rather than apoptotic cell death [57], respectively. However, we did observe strong IHC expression of SPR and NOS in the tumor tissues (Fig. 8A). This strong expression is consistent with mRNA expression and survival data from the SEQC-498 dataset, the largest publicly available RNA sequencing set on NB patient tumors to date. Using Kaplan-Meier analysis, we found that both SPR and NOS1 (nNOS) are widely expressed also in NB tumors, and that their expression is significantly correlated with patient survival: high mRNA expression for either gene is

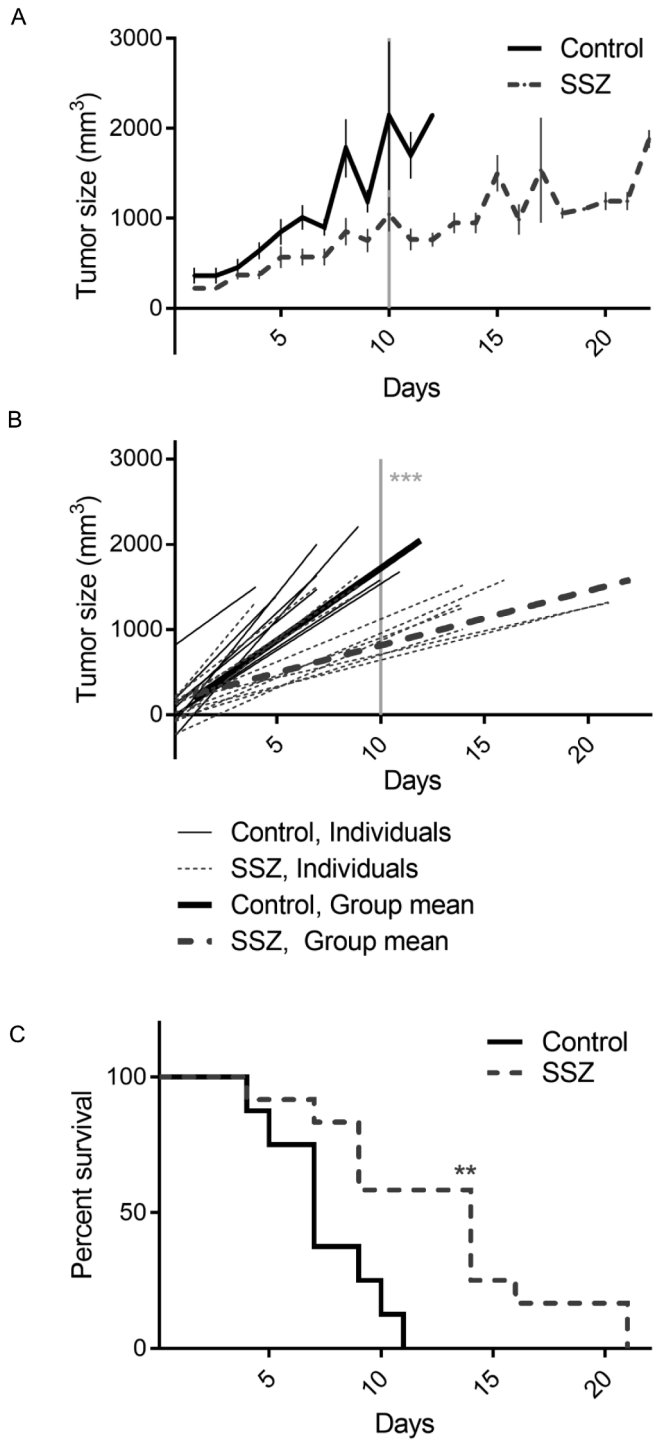

Fig. 6. SSZ reduces the growth rate of NB tumors and improves survival *in vivo*. Xenograft tumors of the NB cell line SKNBE grown subcutaneously in male athymic nu/nu mice. Once palpable tumors became measureable, boxes were assigned to the SSZ treatment (n = 12) or control (n = 8) groups. (A) Tumor sizes were measured three times a week until the 1500 mm^3 threshold for tumor size was surpassed, and animals were euthanized. Last measures were carried forward and average tumor volume ± SEM is displayed. (B) Linear regression fit for tumor sizes within the groups is shown. The mean tumor growth rate was significantly lower in the SSZ treatment group ($F = 35.7$, $^{***}p < 0.001$). (C) Kaplan-Meier survival analysis shows a significant delay in mortality due to tumor size in the SSZ-treated group ($^{**}p < 0.01$).

prognostic for poor outcome (Fig. 8B). The NOS2 (iNOS) and NOS3 (eNOS) genes did not show significant correlations between mRNA tumor expression and patient outcome (not shown). Interestingly, SPR and NOS1/2/3 mRNA expression are positively correlated with statistical significance (Table 2), suggesting a functional link between SPR and NOS gene mRNA expression. Collectively, these data suggest that SPR inhibition and reduced NO production are plausible and clinically relevant targets for SSZ treatment in the context of NB.

4. Discussion

In the current study, we provided first evidence that SSZ inhibits NB tumor growth *in vivo*. The tumor response we observe whereby tumor growth initially decreases upon SSZ treatment, but then recovers later, is similar to the response observed in other cancer models for pancreatic [50] and breast cancer [52]. In addition, we noted some of the NB tumors respond exceptionally well to SSZ treatment, while others do not respond at all and approach control tumor growth, similar to observations in SSZ-treated glioblastoma models [55]. We reiterate that while our observed *in vitro* IC-50 values (~400 μM) would be considered high for most anticancer compounds, the safe clinical use of SSZ in humans ranges from typical daily doses of 1–2 g to a maximal tolerated dose of 12 g for non-cancerous conditions [44]. Maintaining a high dose of SSZ consistently throughout the day appears to be a critical factor in the success of all of the models where SSZ exerts a tumor inhibitory effect *in vivo;* in both our own studies in NB and in a hepatocellular carcinoma model where SSZ was administered only once a day, and no growth inhibition occurred [53]. This appears to be consistent with our *in vitro* studies. In our SKNBE cell lysates, SPR is inhibited with a 2-hour pretreatment, but we did not observe the inhibition with overnight treatment (Fig. 4C). *In vivo*, an additional limitation to our design is the measure of fluid intake per cage (Fig. 5), averaged for the number of animals in the cage, which means we do not know if the responders also drank more intervention than non-responders, or if the ingested dose correlated with other individual signs of toxicity. Despite difficulty achieving sustained tumor growth control with SSZ as a single agent, the studies in pancreatic and hepatocellular carcinoma present promising results when using SSZ as a combination agent with either a cytotoxic compound like etoposide [50] or in conjunction with radiation [53], respectively. Since we have previously observed synergies with SSZ in NB *in vitro* [33], we are optimistic that combination therapy is a promising approach for SSZ in future NB therapy.

SSZ has several known cellular effects that could contribute to our results. We recently identified its target, SPR, and SPR's role in supporting tumor viability in our models of NB [32,33]. We present a model of this new NB vulnerability pathway in Fig. 9, along with some potential effectors. Although SSZ has been observed to suppress NO production by SPR inhibition and lowers cellular proliferation [43], we noted only a weak response in our cell lines. Alternatively, SSZ could increase oxidative stress through suppression of BH4 [58,59] or exacerbate it through inhibition of an additional target: the glutamate-cystine transporter xCT [60,61]. Metabolic depletion of BH4 and cystine uptake and subsequent ROS production contributes to ferroptosis [62,63]. SSZ has been proposed to modulate sensitivity to ferroptosis [64], which would be consistent with our observed tumor suppression despite a lack of caspase cleavage/apoptosis and ki67 proliferation between treated and untreated tumors (Fig. 7). SSZ has also been observed to suppress NF-kB signaling directly by inactivating the IKKα and IKKβ subunits of the NF-kB signaling complex [65], and indirectly through inhibition of upstream inflammatory signaling through the TNFα receptor [66].

While SSZ has been tested in several oncology studies, and was shown to delay tumor progression, its mechanism of action remains controversial. Since SSZ is a pro-drug that is metabolized into two active small molecules (5-ASA and SP), the putative drug activities are

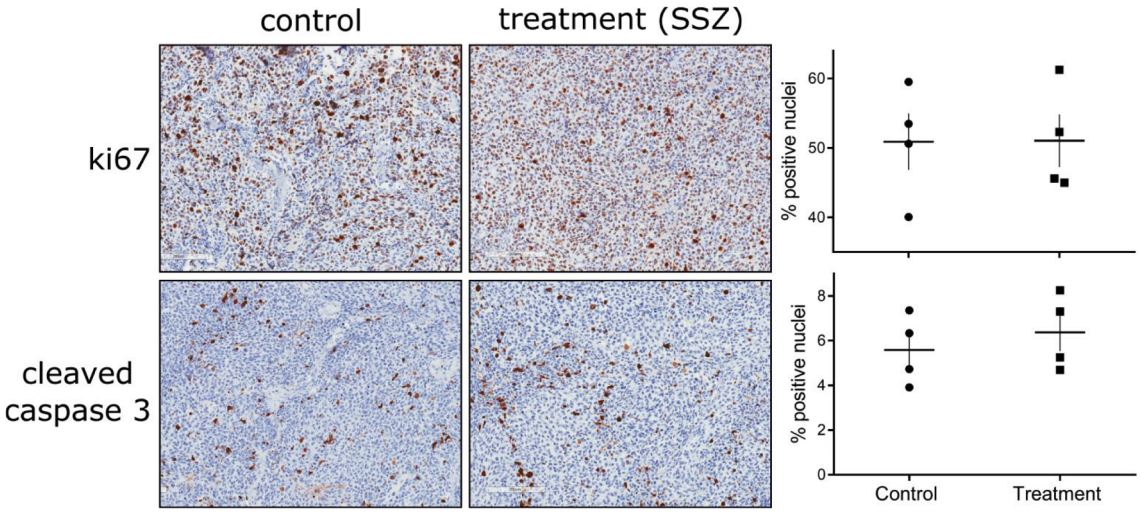

Fig. 7. SSZ does not alter ki67 expression or caspase 3 activation *in vivo*. Tissue sections from treated and untreated tumors were harvested when they reached a threshold size of 1500 mm^3 and stained for ki67 and cleaved caspase 3 to assess whether a reduction in tumor growth rate could be attributed to a lower proliferative index or to cell death. Automatic detection of stained nuclei with Aperio ImageScope software performed on whole tumor regions in 4 tumors from each treatment group did not reveal differences in these markers, consistent with previous reports that SSZ inhibits proliferation without altering ki67 staining [54,56] and affects cell death through non-apoptotic mechanisms [57,64].

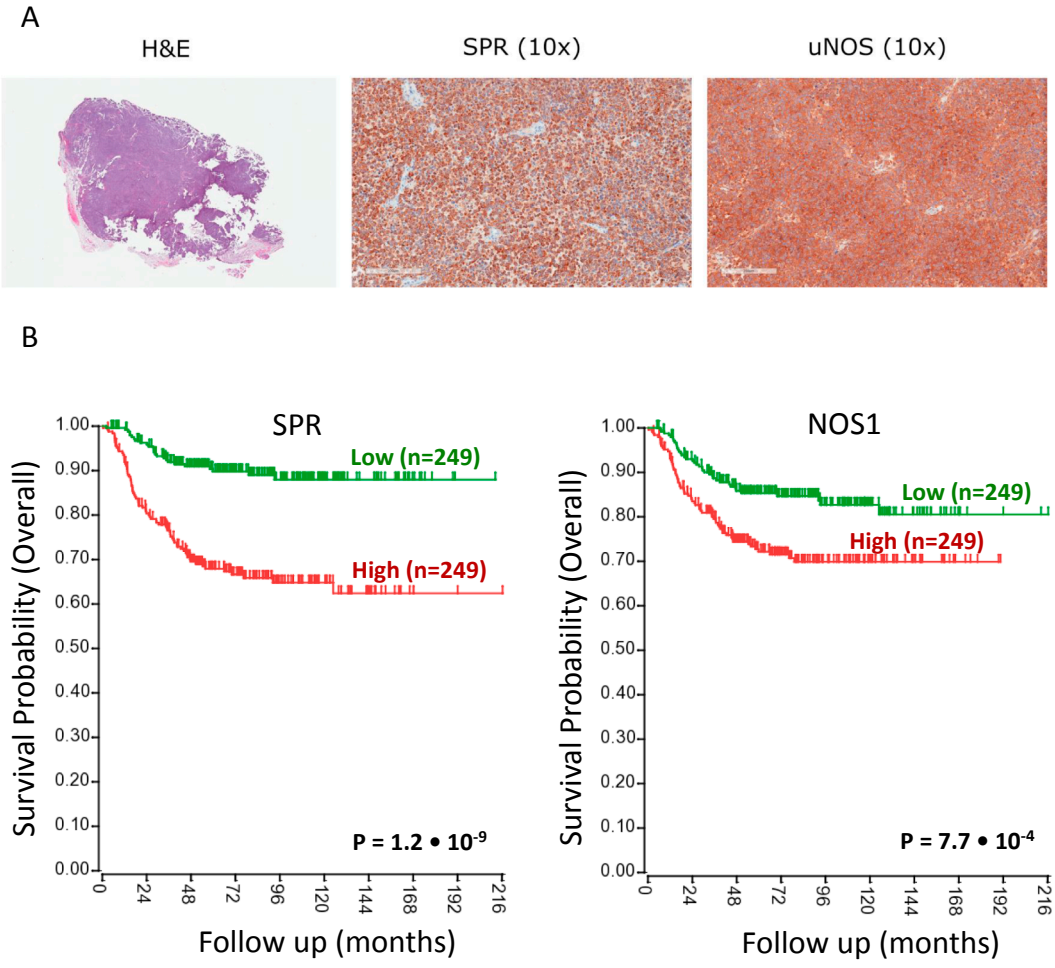

Fig. 8. SPR and NOS are expressed in NB *in vivo*, and high expression correlates with poor patient prognosis. A) Representative IHC pictures of SPR and NOS protein expression in xenograft tumors. (B) RNA expression and survival data from the public SEQC-498 NB dataset; high SPR and NOS1 NB mRNA levels are significantly predictive for poor patient outcome in Kaplan-Meier analysis using median mRNA tumor expression groupings (see Materials and Methods). The results shown are for overall patient survival.

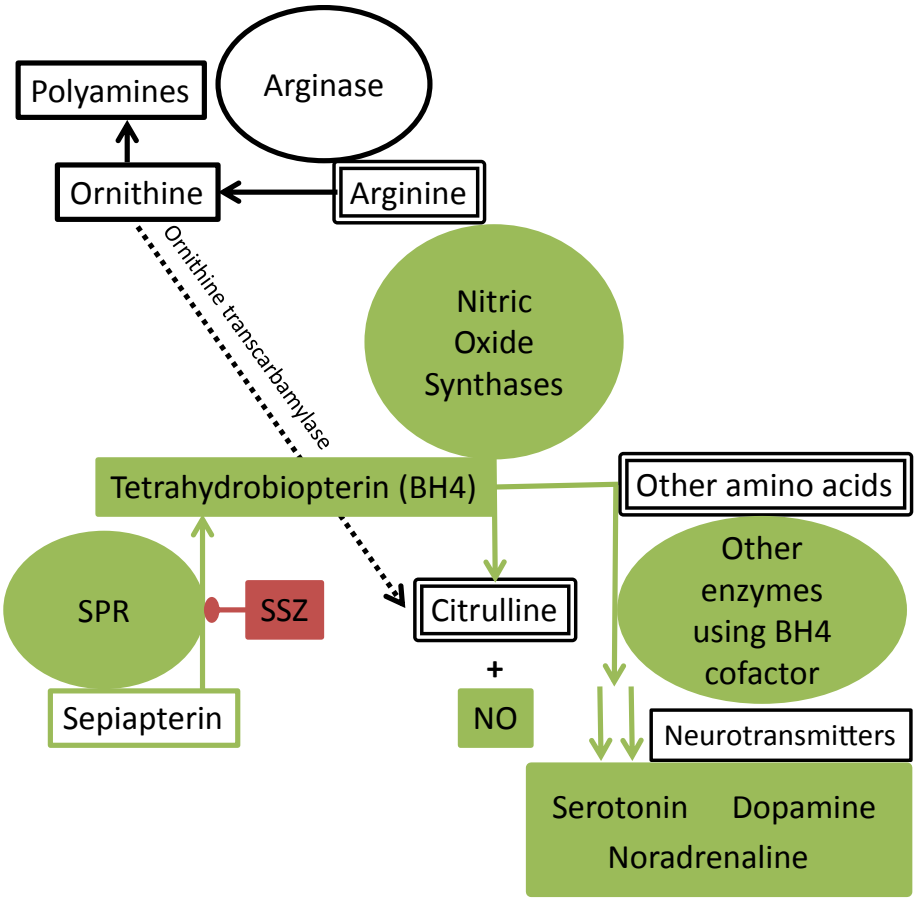

Fig. 9. Model of anti-tumor effects of SSZ through SPR. SPR in NB contributes to tumor growth and survival through pleiotropic cellular effects that supply amino acid metabolism through the production of the enzymatic cofactor tetrahydrobiopterin (BH4). In the model, SSZ inhibits SPR activity to normalize cell metabolism. Circles represent enzymes, boxes represent small molecules, and double boxes are α-amino acids. Enzymes act on the small molecules in the boxes or connected to the lines they touch. Black, physiologic metabolism; green, pathologic SPR in NB; red, small molecule inhibitor. Sulfasalazine, SSZ; Sepiapterin Reductase, SPR; NO, Nitric Oxide.

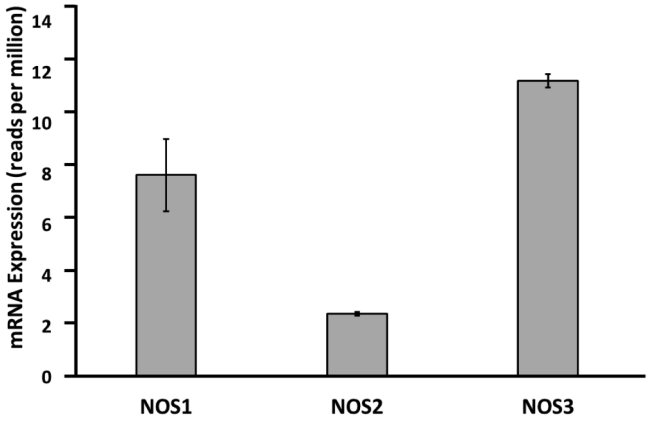

Fig. 10. Nitric oxide synthase gene mRNA expression in NB tumors. The SEQC-498 RNASeq NB tumor dataset was queried for nitric oxide synthase (NOS) gene expression. The graph shows average expression (in reads per million) for the predominant mRNA splice variants for each gene: NOS1 (NM_000620.4, isoform 1), NOS2 (NM_000625.4), NOS3 (NM_000603.4, isoform 1). NOS1 and NOS3 are the highest expressed NOS genes in NB. For details on dataset analysis see Materials and Methods. Error bars indicate standard deviation.

diverse, and include immune suppression, anti-inflammatory effects, lipo- and cyclo-oxygenase inhibition, NF-kB inhibition, inhibition of the glutamate transporter xCT, and, most recently, inhibition of the enzyme SPR. Immune suppression [67], the anti-inflammatory effects [68], and lipo- and cyclo-oxygenase inhibition [69], are the best known effects of SSZ and are produced by the 5-ASA moiety, which is not absorbed through the intestinal tract [45,46], and are not typically the activities examined in an oncogenic context. Instead, inhibition of both NF-kB and xCT putatively rely on an intact SSZ compound, rather than either of the metabolites, and have been discussed more widely as potential mechanisms for SSZ's anti-cancer effects [65,70]. While the role of NF-kB in cancer is complex, it is usually tumor-protective by suppressing apoptosis, including in NB [71]. While SSZ has been shown to inhibit NF-kB in pancreatic xenografts [50], the effect was not replicated in other cancer types like gliomas, where SSZ exerts NF-kB-independent effects on xenografts [72]. In this glioma study, as well as in a later pancreatic cancer study, inhibition of the xCT transporter system has been considered instead. However, both NF-kB and xCT inhibition appear to rely on an intact SSZ compound, only 10–25% of which is absorbed in the small intestine [45,46]. Another new target for SSZ is SPR inhibition, which can be mediated either by the un-metabolized SSZ compound or by the SP metabolite [18], the latter of which is absorbed nearly completely from the colon. In this study we present further evidence that SPR is well expressed in NB and is a significant predictor for poor outcome, that SSZ inhibits SPR and trends toward suppression of NO, and that SSZ administration as a single agent reduces NB tumor growth rates. The relative impacts of SSZ on the NF-kB, xCT, and SPR molecular pathways await further study.

Although we were unable to show significant suppression of induced NO production by SPR inhibition, the mechanism is most probably active in NB cells; mRNA expression analysis of the SEQC-498 dataset showed that the constitutive NOS1 and NOS3 genes are higher expressed than the inducible NOS2 gene (Fig. 10), and could drown the SSZ effect on NOS2 in SKNBE cells.

In summary, SPR is a target of the FDA-approved drug SSZ. SPR is well expressed in NB, and NB cells are sensitive to SSZ both *in vitro* and *in vivo*, where we observe anti-proliferative effects. SSZ could be repositioned to inhibit NB tumor growth and represent an opportune compound either for use in a combination therapy or as a subject for the generation of chemical analogs or re-formulations to achieve more potency. Similar to DFMO, the use of SSZ in the chemoprevention

setting may also be considered given its moderate toxicity profile and its well-established long-term use for patients with ulcerative colitis.

Author contributions

ASB conceived and designed the study, MRM, DG, and EJK developed the methodology, MRM, DG, and EJK conducted the experiments and collected the data, MRM and DG performed data analysis, and MRM, DG, EJK, and ASB wrote and finalized the manuscript. All authors approved the final version for publication.

Conflict of interest

The authors declare no conflict of interest.

Acknowledgments

This work was supported by the Wipe Out Kids' Cancer (WOKC) Foundation in Dallas, TX to ASB and MSU-internal discretionary funds to ASB. We thank Chad R. Schultz (MSU Department of Pediatrics and Human Development) for his expert technical support and scientific discussions throughout this study. We also thank Dr. David Monsma and his staff (Preclinical Therapeutics Core Service, Van Andel Research Institute) for providing guidance and technical assistance on the *in vivo* studies, and Zach Madaj (Biostatistics Core, Van Andel Research Institute) for consultation on statistical measures for the *in vivo* study. The authors wish to thank Jan Koster (Department of Oncogenomics at the Academic Medical Center Amsterdam) for access to and advice on R2. We are also grateful for the kind provision of cell lines from Dr. Jason Shohet (Texas Children's Cancer Center, Baylor College of Medicine, Houston, TX) and Dr. Manfred Schwab (German Cancer Research Center DKFZ, Heidelberg, Germany).

References

[1] C.U. Louis, J.M. Shohet, Neuroblastoma: molecular pathogenesis and therapy, Annu. Rev. Med. 66 (2015) 49–63.
[2] J.M. Maris, Recent advances in neuroblastoma, New Engl. J. Med. 362 (23) (2010) 2202–2211.
[3] K.K. Matthay, J.M. Maris, G. Schleiermacher, A. Nakagawara, C.L. Mackall, L. Diller, W.A. Weiss, Neuroblastoma, Nat. Rev. Dis. Primers 2 (2016) 16078.
[4] M.F. Ozkaynak, A.L. Gilman, W.B. London, A. Naranjo, M.B. Diccianni, S.C. Tenney, M. Smith, K.S. Messer, R. Seeger, C.P. Reynolds, L.M. Smith, B.L. Shulkin, M. Parisi, J.M. Maris, J.R. Park, P.M. Sondel, A.L. Yu, A Comprehensive safety trial of chimeric antibody 14.18 with GM-CSF, IL-2, and isotretinoin in high-risk neuroblastoma patients following myeloablative therapy: Children's Oncology Group Study ANBL0931, Front. Immunol. 9 (2018) 1355.
[5] R. Bagatell, S.L. Cohn, Genetic discoveries and treatment advances in neuroblastoma, Curr. Opin. Pediatr. 28 (1) (2016) 19–25.
[6] C.J. Wallick, I. Gamper, M. Thorne, D.J. Feith, K.Y. Takasaki, S.M. Wilson, J.A. Seki, A.E. Pegg, C.V. Byus, A.S. Bachmann, Key role for p27Kip1, retinoblastoma protein Rb, and MYCN in polyamine inhibitor-induced G1 cell cycle arrest in MYCN-amplified human neuroblastoma cells, Oncogene 24 (36) (2005) 5606–5618.
[7] D.-L.T. Koomoa, L.P. Yco, T. Borsics, C.J. Wallick, A.S. Bachmann, Ornithine decarboxylase inhibition by alpha-difluoromethylornithine activates opposing signaling pathways via phosphorylation of both Akt/protein kinase B and p27Kip1 in neuroblastoma, Cancer Res. 68 (23) (2008) 9825–9831.
[8] A.S. Bachmann, D. Geerts, G.L. Saulnier Sholler, Neuroblastoma: ornithine decarboxylase and polyamines are novel targets for therapeutic intervention, in: M.A. Hayat (Ed.), Neuroblastoma: Diagnosis, Therapy, and Prognosis, Springer, Netherlands, Dordrecht, 2012, pp. 91–103.
[9] D.-L.T. Koomoa, D. Geerts, I. Lange, J. Koster, A.E. Pegg, D.J. Feith, A.S. Bachmann, DFMO/eflornithine inhibits migration and invasion downstream of MYCN and involves p27Kip1 activity in neuroblastoma, Int. J. Oncol. 42 (4) (2013) 1219–1228.
[10] G.L.S. Sholler, E.W. Gerner, G. Bergendahl, R.B. MacArthur, A. VanderWerff, T. Ashikaga, J.P. Bond, W. Ferguson, W. Roberts, R.K. Wada, D. Eslin, J.M. Kraveka, J. Kaplan, D. Mitchell, N.S. Parikh, K. Neville, L. Sender, T. Higgins, M. Kawakita, K. Hiramatsu, S.-S. Moriya, A.S. Bachmann, A phase I trial of DFMO targeting polyamine addiction in patients with relapsed/refractory neuroblastoma, PLoS One 10 (5) (2015) e0127246.
[11] C.R. Schultz, D. Geerts, M. Mooney, R. El-Khawaja, J. Koster, A.S. Bachmann, Synergistic drug combination GC7/DFMO suppresses hypusine/spermidine-dependent eIF5A activation and induces apoptotic cell death in neuroblastoma, Biochem. J. 475 (2) (2018) 531–545.
[12] A.S. Bachmann, The role of polyamines in human cancer: prospects for drug combination therapies, Hawaii Med. J. 63 (12) (2004) 371–374.
[13] A.S. Bachmann, D. Geerts, Polyamine synthesis as a target of MYC oncogenes, J. Biol. Chem. 293 (48) (2018) 18757–18769.
[14] D. Geerts, J. Koster, D. Albert, D.L. Koomoa, D.J. Feith, A.E. Pegg, R. Volckmann, H. Caron, R. Versteeg, A.S. Bachmann, The polyamine metabolism genes ornithine decarboxylase and antizyme 2 predict aggressive behavior in neuroblastomas with and without MYCN amplification, Int. J. Cancer 126 (9) (2010) 2012–2024.
[15] C.P. Rains, S. Noble, D. Faulds, Sulfasalazine. A review of its pharmacological properties and therapeutic efficacy in the treatment of rheumatoid arthritis, Drugs 50 (1) (1995) 137–156.
[16] A.I. Jacknowitz, Ulcerative colitis and its treatment, Am. J. Hospital Pharmacy 37 (12) (1980) 1635–1646.
[17] N. Svartz, Salazopyrin, a new sulfanilamide preparation. A. Therapeutic results in rheumatic polyarthritis. B. Therapeutic results in ulcerative colitis. C. Toxic manifestations in treatment with sulfanilamide preparations, Acta Med. Scand. 110 (6) (1942) 577–598.
[18] H. Haruki, M.G. Pedersen, K.I. Gorska, F. Pojer, K. Johnsson, Tetrahydrobiopterin biosynthesis as an off-target of sulfa drugs, Science (New York, N.Y.) 340 (6135) (2013) 987–991.
[19] L. Chen, X. Zeng, J. Wang, S.S. Briggs, E. O'Neill, J. Li, R. Leek, D.J. Kerr, A.L. Harris, S. Cai, Roles of tetrahydrobiopterin in promoting tumor angiogenesis, Am. J. Pathol. 177 (5) (2010) 2671–2680.
[20] P.Z. Anastasiadis, J.C. States, B.A. Imerman, M.C. Louie, D.M. Kuhn, R.A. Levine, Mitogenic effects of tetrahydrobiopterin in PC12 cells, Mol. Pharmacol. 49 (1) (1996) 149–155.
[21] Y.-R. Cho, S.W. Choi, D.-W. Seo, Sepiapterin regulates cell proliferation and migration: its association with integrin α3β1 and p53 in human lung cancer cells, Genes Genomics 33 (5) (2011) 577.
[22] Y.-R. Cho, S.H. Kim, H.Y. Ko, M.-D. Kim, S.W. Choi, D.-W. Seo, Sepiapterin inhibits cell proliferation and migration of ovarian cancer cells via down-regulation of p70S6K-dependent VEGFR-2 expression, Oncol. Rep. 26 (4) (2011) 861–867.
[23] T. Shang, S. Kotamraju, H. Zhao, S.V. Kalivendi, C.J. Hillard, B. Kalyanaraman, Sepiapterin attenuates 1-methyl-4-phenylpyridinium-induced apoptosis in neuroblastoma cells transfected with neuronal NOS: role of tetrahydrobiopterin, nitric oxide, and proteasome activation, Free Radical Biol. Med. 39 (8) (2005) 1059–1074.
[24] M. Murillo-Carretero, M.J. Ruano, E.R. Matarredona, A. Villalobo, C. Estrada, Antiproliferative effect of nitric oxide on epidermal growth factor-responsive human neuroblastoma cells, J. Neurochem. 83 (1) (2002) 119–131.
[25] R. Moriya, T. Uehara, Y. Nomura, Mechanism of nitric oxide-induced apoptosis in human neuroblastoma SH-SY5Y cells, FEBS Lett. 484 (3) (2000) 253–260.
[26] D.D. Thomas, L.A. Ridnour, J.S. Isenberg, W. Flores-Santana, C.H. Switzer, S. Donzelli, P. Hussain, C. Vecoli, N. Paolocci, S. Ambs, C.A. Colton, C.C. Harris, D.D. Roberts, D.A. Wink, The chemical biology of nitric oxide: implications in cellular signaling, Free Radical Biol. Med. 45 (1) (2008) 18–31.
[27] E. Junn, M.M. Mouradian, Apoptotic signaling in dopamine-induced cell death: the role of oxidative stress, p38 mitogen-activated protein kinase, cytochrome c and caspases, J. Neurochem. 78 (2) (2001) 374–383.
[28] L. Jiang, N. Kon, T. Li, S.-J. Wang, T. Su, H. Hibshoosh, R. Baer, W. Gu, Ferroptosis as a p53-mediated activity during tumour suppression, Nature 520 (7545) (2015) 57–62.
[29] M.G. Nashed, R.G. Ungard, K. Young, N.J. Zacal, E.P. Seidlitz, J. Fazzari, B.N. Frey, G. Singh, Behavioural effects of using sulfasalazine to inhibit glutamate released by cancer cells: a novel target for cancer-induced depression, Sci. Rep. 7 (2017) 41382.
[30] H. Sontheimer, R.J. Bridges, Sulfasalazine for brain cancer fits, Expert Opin. Invest. Drugs 21 (5) (2012) 575–578.
[31] A. Latremoliere, A. Latini, N. Andrews, S.J. Cronin, M. Fujita, K. Gorska, R. Hovius, C. Romero, S. Chuaiphichai, M. Painter, G. Miracca, O. Babaniyi, A.P. Remor, K. Duong, P. Riva, L.B. Barrett, N. Ferreirós, A. Naylor, J.M. Penninger, I. Tegeder, J. Zhong, J. Blagg, K.M. Channon, K. Johnsson, M. Costigan, C.J. Woolf, Reduction of neuropathic and inflammatory pain through inhibition of the tetrahydrobiopterin pathway, Neuron 86 (6) (2015) 1393–1406.
[32] I. Lange, D. Geerts, D.J. Feith, G. Mocz, J. Koster, A.S. Bachmann, Novel interaction of ornithine decarboxylase with sepiapterin reductase regulates neuroblastoma cell proliferation, J. Mol. Biol. 426 (2) (2014) 332–346.
[33] L.P. Yco, D. Geerts, G. Mocz, J. Koster, A.S. Bachmann, Effect of sulfasalazine on human neuroblastoma: analysis of sepiapterin reductase (SPR) as a new therapeutic target, BMC Cancer 15 (2015) 477.
[34] A. Slack, Z. Chen, R. Tonelli, M. Pule, L. Hunt, A. Pession, J.M. Shohet, The p53 regulatory gene MDM2 is a direct transcriptional target of MYCN in neuroblastoma, PNAS 102 (3) (2005) 731–736.
[35] W. Lutz, M. Stohr, J. Schurmann, A. Wenzel, A. Lohr, M. Schwab, Conditional expression of N-myc in human neuroblastoma cells increases expression of alpha-prothymosin and ornithine decarboxylase and accelerates progression into S-phase early after mitogenic stimulation of quiescent cells, Oncogene 13 (4) (1996) 803–812.
[36] A. Latremoliere, A. Latini, N. Andrews, S.J. Cronin, M. Fujita, K. Gorska, R. Hovius, C. Romero, S. Chuaiphichai, M. Painter, G. Miracca, O. Babaniyi, A.P. Remor, K. Duong, P. Riva, L.B. Barrett, N. Ferreiros, A. Naylor, J.M. Penninger, I. Tegeder, J. Zhong, J. Blagg, K.M. Channon, K. Johnsson, M. Costigan, C.J. Woolf, Reduction of neuropathic and inflammatory pain through inhibition of the tetrahydrobiopterin pathway, Neuron 86 (2015) 1393–1406.
[37] M. Fischer, M. Skowron, F. Berthold, Reliable transcript quantification by real-time reverse transcriptase-polymerase chain reaction in primary neuroblastoma using normalization to averaged expression levels of the control genes HPRT1 and SDHA, J. Mol. Diagnostics: JMD 7 (1) (2005) 89–96.

[38] I. Revet, G. Huizenga, A. Chan, J. Koster, R. Volckmann, P. van Sluis, I. Øra, R. Versteeg, D. Geerts, The MSX1 homeobox transcription factor is a downstream target of PHOX2B and activates the Delta-Notch pathway in neuroblastoma, Exp. Cell Res. 314 (4) (2008) 707–719.
[39] V. Bewick, L. Cheek, J. Ball, Statistics review 12: survival analysis, Crit Care 8 (5) (2004) 389–394.
[40] M.G. Pedersen, F. Pojer, K. Johnsson, 4J7X: Crystal Structure Of Human Sepiapterin Reductase In Complex With Sulfasalazine. https://www.rcsb.org/structure/4J7X.
[41] A. Grosdidier, V. Zoete, O. Michielin, SwissDock, a protein-small molecule docking web service based on EADock DSS, Nucleic Acids Res. 39 (Web Server issue) (2011) W270-7.
[42] G. Auerbach, A. Herrmann, M. Gütlich, M. Fischer, U. Jacob, A. Bacher, R. Huber, The 1.25 A crystal structure of sepiapterin reductase reveals its binding mode to pterins and brain neurotransmitters, EMBO J. 16 (24) (1997) 7219–7230.
[43] K. Tanaka, S. Kaufman, S. Milstien, Tetrahydrobiopterin, the cofactor for aromatic amino acid hydroxylases, is synthesized by and regulates proliferation of erythroid cells, PNAS 86 (15) (1989) 5864–5867.
[44] S.R. Feldman, K.C. Phelps, K.C. Verzino, Handbook of Dermatologic Drug Therapy, CRC Press, 2005.
[45] W. Zheng, S.M. Winter, M. Mayersohn, J.B. Bishop, I.G. Sipes, Toxicokinetics of sulfasalazine (salicylazosulfapyridine) and its metabolites in B6C3F1 mice, Drug Metab. Dispos. 21 (6) (1993) 1091–1097.
[46] M.A. Peppercorn, Sulfasalazine. Pharmacology, clinical use, toxicity, and related new drug development, Ann. Internal Med. 101 (3) (1984) 377–386.
[47] M. Diculescu, M. Ciocîrlan, M. Ciocîrlan, D. Piţigoi, G. Becheanu, A. Croitoru, S. Spanache, Folic acid and sulfasalazine for colorectal carcinoma chemoprevention in patients with ulcerative colitis: the old and new evidence, Romanian J. Gastroenterol. 12 (4) (2003) 283–286.
[48] K. Shitara, T. Doi, O. Nagano, C.K. Imamura, T. Ozeki, Y. Ishii, K. Tsuchihashi, S. Takahashi, T.E. Nakajima, S. Hironaka, M. Fukutani, H. Hasegawa, S. Nomura, A. Sato, Y. Einaga, T. Kuwata, H. Saya, A. Ohtsu, Dose-escalation study for the targeting of CD44v+ cancer stem cells by sulfasalazine in patients with advanced gastric cancer (EPOC1205), Gastric Cancer 20 (2) (2017) 341–349.
[49] D.W. Doxsee, P.W. Gout, T. Kurita, M. Lo, A.R. Buckley, Y. Wang, H. Xue, C.M. Karp, J.-C. Cutz, G.R. Cunha, Y.-Z. Wang, Sulfasalazine-induced cystine starvation: potential use for prostate cancer therapy, Prostate 67 (2) (2007) 162–171.
[50] S. Müerköster, A. Arlt, M. Witt, A. Gehrz, S. Haye, C. March, F. Grohmann, K. Wegehenkel, H. Kalthoff, U.R. Fölsch, H. Schäfer, Usage of the NF-kappaB inhibitor sulfasalazine as sensitizing agent in combined chemotherapy of pancreatic cancer, Int. J. Cancer 104 (4) (2003) 469–476.
[51] M. Lo, V. Ling, C. Low, Y.Z. Wang, P.W. Gout, Potential use of the anti-inflammatory drug, sulfasalazine, for targeted therapy of pancreatic cancer, Curr. Oncol. (Toronto, Ont.) 17 (3) (2010) 9–16.
[52] L.A. Timmerman, T. Holton, M. Yuneva, R.J. Louie, M. Padró, A. Daemen, M. Hu, D.A. Chan, S.P. Ethier, L.J. van 't Veer, K. Polyak, F. McCormick, J.W. Gray, Glutamine sensitivity analysis identifies the xCT antiporter as a common triple-negative breast tumor therapeutic target, Cancer Cell 24 (4) (2013) 450–465.
[53] Y. Song, J. Jang, T.-H. Shin, S.M. Bae, J.-S. Kim, K.M. Kim, S.-J. Myung, E.K. Choi, H.R. Seo, Sulfasalazine attenuates evading anticancer response of CD133-positive hepatocellular carcinoma cells, J. Exp. Clin. Cancer Res.: CR 36 (1) (2017) 38.
[54] W.J. Chung, S.A. Lyons, G.M. Nelson, H. Hamza, C.L. Gladson, G.Y. Gillespie, H. Sontheimer, Inhibition of cystine uptake disrupts the growth of primary brain tumors, J. Neurosci. 25 (31) (2005) 7101–7110.
[55] P.A. Robe, M. Bentires-Alj, M. Bonif, B. Rogister, M. Deprez, H. Haddada, M.-T.N. Khac, O. Jolois, K. Erkmen, M.-P. Merville, P.M. Black, V. Bours, In vitro and in vivo activity of the nuclear factor-kappaB inhibitor sulfasalazine in human glioblastomas, Clinical Cancer Res. 10 (16) (2004) 5595–5603.
[56] P. Sharon, E.A. Drab, J.S. Linder, S.W. Weidman, S.M. Sabesin, D.B. Rubin, The effect of sulfasalazine on bovine endothelial cell proliferation and cell cycle phase distribution. Comparison with olsalazine, 5-aminosalicylic acid, and sulfapyridine, J. Lab. Clin. Med. 119 (1) (1992) 99–107.
[57] T. Sehm, Z. Fan, A. Ghoochani, M. Rauh, T. Engelhorn, G. Minakaki, A. Dörfler, J. Klucken, M. Buchfelder, I.Y. Eyüpoglu, N. Savaskan, Sulfasalazine impacts on ferroptotic cell death and alleviates the tumor microenvironment and glioma-induced brain edema, Oncotarget 7 (24) (2016) 36021–36033.
[58] L.M. Bevers, B. Braam, J.A. Post, A.J. van Zonneveld, T.J. Rabelink, H.A. Koomans, M.C. Verhaar, J.A. Joles, Tetrahydrobiopterin, but not L-arginine, decreases NO synthase uncoupling in cells expressing high levels of endothelial NO synthase, Hypertension (Dallas, Tex.: 1979) 47 (1) (2006) 87–94.
[59] M.P. Brand, S.J. Heales, J.M. Land, J.B. Clark, Tetrahydrobiopterin deficiency and brain nitric oxide synthase in the hph1 mouse, J. Inherit. Metab. Dis. 18 (1) (1995) 33–39.
[60] P.W. Gout, A.R. Buckley, C.R. Simms, N. Bruchovsky, Sulfasalazine, a potent suppressor of lymphoma growth by inhibition of the x(c)-cystine transporter: a new action for an old drug, Leukemia 15 (10) (2001) 1633–1640.
[61] X. Ji, J. Qian, S.M.J. Rahman, P.J. Siska, Y. Zou, B.K. Harris, M.D. Hoeksema, I.A. Trenary, C. Heidi, R. Eisenberg, J.C. Rathmell, J.D. Young, P.P. Massion, xCT (SLC7A11)-mediated metabolic reprogramming promotes non-small cell lung cancer progression, Oncogene (2018).
[62] S.J. Dixon, K.M. Lemberg, M.R. Lamprecht, R. Skouta, E.M. Zaitsev, C.E. Gleason, D.N. Patel, A.J. Bauer, A.M. Cantley, W.S. Yang, B. Morrison, B.R. Stockwell, Ferroptosis: an iron-dependent form of nonapoptotic cell death, Cell 149 (5) (2012) 1060–1072.
[63] E.H. Kim, D. Shin, J. Lee, A.R. Jung, J.L. Roh, CISD2 inhibition overcomes resistance to sulfasalazine-induced ferroptotic cell death in head and neck cancer, Cancer Lett. 432 (2018) 180–190.
[64] B.R. Stockwell, J.P. Friedmann Angeli, H. Bayir, A.I. Bush, M. Conrad, S.J. Dixon, S. Fulda, S. Gascon, S.K. Hatzios, V.E. Kagan, K. Noel, X. Jiang, A. Linkermann, M.E. Murphy, M. Overholtzer, A. Oyagi, G.C. Pagnussat, J. Park, Q. Ran, C.S. Rosenfeld, K. Salnikow, D. Tang, F.M. Torti, S.V. Torti, S. Toyokuni, K.A. Woerpel, D.D. Zhang, Ferroptosis: a regulated cell death nexus linking metabolism, redox biology, and disease, Cell 171 (2) (2017) 273–285.
[65] C.K. Weber, S. Liptay, T. Wirth, G. Adler, R.M. Schmid, Suppression of NF-kappaB activity by sulfasalazine is mediated by direct inhibition of IkappaB kinases alpha and beta, Gastroenterology 119 (5) (2000) 1209–1218.
[66] F. Shanahan, A. Niederlehner, N. Carramanzana, P. Anton, Sulfasalazine inhibits the binding of TNF alpha to its receptor, Immunopharmacology 20 (3) (1990) 217–224.
[67] R.P. MacDermott, S.R. Schloemann, M.J. Bertovich, G.S. Nash, M. Peters, W.F. Stenson, Inhibition of antibody secretion by 5-aminosalicylic acid, Gastroenterology 96 (2 Pt 1) (1989) 442–448.
[68] D. Rachmilewitz, F. Karmeli, L.W. Schwartz, P.L. Simon, Effect of aminophenols (5-ASA and 4-ASA) on colonic interleukin-1 generation, Gut 33 (7) (1992) 929–932.
[69] C.J. Hawkey, N.K. Boughton-Smith, B.J. Whittle, Modulation of human colonic arachidonic acid metabolism by sulfasalazine, Dig. Dis. Sci. 30 (12) (1985) 1161–1165.
[70] P.W. Gout, C.R. Simms, M.C. Robertson, In vitro studies on the lymphoma growth-inhibitory activity of sulfasalazine, Anticancer Drugs 14 (1) (2003) 21–29.
[71] L. Wang, B.-F. Cheng, H.-J. Yang, M. Wang, Z.-W. Feng, NF-κB protects human neuroblastoma cells from nitric oxide-induced apoptosis through upregulating biglycan, Am. J. Trans. Res. 7 (9) (2015) 1541–1552.
[72] W.J. Chung, H. Sontheimer, Sulfasalazine inhibits the growth of primary brain tumors independent of nuclear factor-kappaB, J. Neurochem. 110 (1) (2009) 182–193.